

# Digital Controllers in Discrete and Continuous Time Domains for a Robot Arm Manipulator

1<sup>st</sup> Dhiman Chowdhury, *Student Member, IEEE*  
 Electrical Engineering  
 University of South Carolina  
 Columbia, South Carolina, USA  
 dhiman@email.sc.edu

2<sup>nd</sup> Mrinmoy Sarkar, *Student Member, IEEE*  
 Electrical and Computer Engineering  
 North Carolina A & T State University  
 Greensboro, NC 27411, USA  
 msarkar@aggies.ncat.edu

**Abstract**—This paper articulates design and performance analysis of digital controllers in discrete and continuous time domains for a single-joint robot arm manipulator. The investigated robot arm system is modeled as a single degree of freedom (DOF) plant and there is a feedback sensor implying a closed-loop system. The design approach incorporates discrete (z-plane) and continuous time (warped s-plane or w-plane) domain parameters. Four digital controllers - phase-lag, phase-lead, proportional-integral (PI) and proportional-integral-derivative (PID) are theoretically designed and implemented to achieve a phase margin of 40 deg. for the compensated system. For performance evaluations, Bode plots of the compensated open-loop systems and step response characteristics of the closed-loop systems are determined.

**Index Terms**—Bode plot, controllers, continuous time, discrete, phase margin, robot arm manipulator, step response

## I. INTRODUCTION

Controllers are essential to determine the changes of system parameters and to attain desired characteristics with performance specifications, which are related to steady-state accuracy, transient response, stability and disturbance reduction [1]. Analog controllers are hard to synthesize complicated logics, to make dynamic interfaces among multiple subsystems and are highly susceptible to corruption by extraneous noise sources [1]. However, digital controllers are reliable, since no signal loss occurs in analog-to-digital (A/D) and digital-to-analog (D/A) conversions and are more flexible and accurate in case of sophisticated logic implementation [1]. In addition, digital controllers are not subject to external noises. Several applications of digital control algorithms in robotics and automated systems are reported in [1] - [5].

This paper documents design methodologies of different types of digital controllers - phase-lag, phase-lead, proportional-integral (PI) and proportional-integral-derivative (PID) for a physical system of a single DOF robot arm manipulator. Phase margin is compensated in the system employing cross-over frequency as the primary design parameter. Bode diagrams of the open-loop systems and step response characteristics of the closed-loop systems are determined. Comparative analysis of the designed controllers is carried out. MATLAB® simulations are applied for the proposed framework. However, several works on robot arm systems for efficient control phenomena are articulated in [6] - [10].

The major contributions of this research paper are to -  
 a. conceptualize digital controllers in discrete and continuous time domains for a single-joint robot arm manipulator.  
 b. design controllers for a particular compensation criterion (phase margin) using frequency response techniques.  
 c. derive Bode plots and step responses of the compensated systems and compare the characteristics obtained from different controllers.

The remainder of this manuscript is organized as follows. Section II documents the investigated robot arm system, plant transfer function and basic compensation theory of the digital controllers. Sections III - VI describe the design methodologies of phase-lag, phase-lead, PI and PID controllers, respectively. Section VII presents the step response characteristics. Section VIII concludes the paper.

## II. ROBOT ARM SYSTEM, PLANT TRANSFER FUNCTION AND DIGITAL CONTROLLER

Fig. 1 presents the block diagram of the investigated single joint (1-DOF) robot arm manipulator system. The plant configuration follows the mathematical modeling approach reported in [6] - [7]. Here the sampling time is  $T_s = 0.1$  s and the potentiometer constant  $K_{pot} = \frac{V_p}{\theta_a} = \frac{12-0}{180-0} = 0.0667$  V/deg. However, the compensation theory, corresponding mathematical derivations for the controller design and open loop and closed loop parameters of the controllers described in this paper follow the literature documented in [1]. According to [1], for a first-order compensation, the controller transfer function can be expressed as  $D(z) = \frac{K_d(z-z_0)}{z-z_p}$ . Here  $z_0$  and  $z_p$  are the respective zero and pole locations. The bilinear or trapezoidal

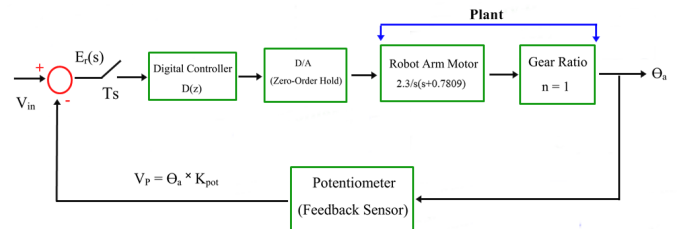


Fig. 1. Block diagram of the robot arm manipulator system

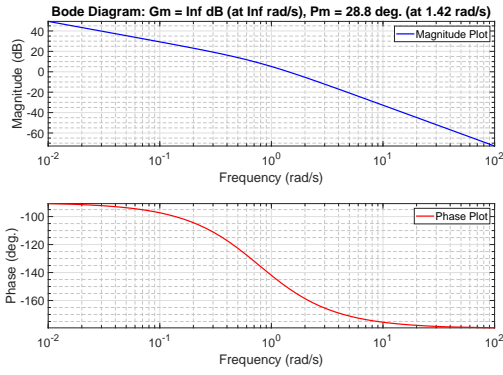


Fig. 2. Bode plot of the uncompensated plant (robot arm motor + gear)

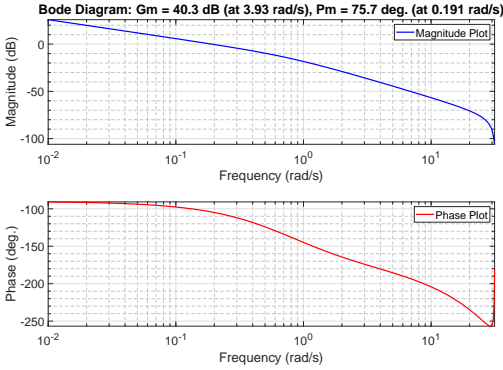


Fig. 3. Bode plot of the plant + feedback sensor (uncompensated open-loop system)

transformation of the controller from the discrete  $z$ -plane to the continuous  $w$ -plane (warped  $s$ -plane) implies  $D(w) = D(z)$ ,  $z = \frac{1+(T/2)w}{1-(T/2)w}$ , such that  $D(w) = a_0 \frac{1+(w/\omega_{w0})}{1+(w/\omega_{wp})}$ . Here  $\omega_{w0}$  and  $\omega_{wp}$  are the respective zero and pole locations in the  $w$ -plane and  $a_0$  is the compensator DC gain. According to the bilinear approximation,  $w = \frac{2}{T} \frac{z-1}{z+1}$ . From the above equations, in  $z$ -plane the controller can be realized as

$$D(z) = a_0 \frac{\omega_{wp}(\omega_{w0} + 2/T)}{\omega_{w0}(\omega_{wp} + 2/T)} \frac{z - (2/T - \omega_{w0})}{z - (2/T - \omega_{wp})} \quad (1)$$

For the uncompensated plant, the controller,  $D(z) = 1$ . The zero-order hold transfer function can be defined as  $G_{HO}(s) = \frac{1-e^{-sT}}{s}$ . The continuous-time plant with feedback sensor gain transfer function,  $G_c(s) = \frac{0.1533}{s^2+0.7809s}$ . The discrete-time plant with feedback sensor gain transfer function is

$$G_d(z) = \frac{0.0007471z + 0.0007279}{z^2 - 1.925z + 0.9249} \quad (2)$$

Figs. 2 and 3 present the Bode plots of the plant and uncompensated plant + feedback sensor system, respectively.

### III. PHASE-LAG CONTROLLER DESIGN

The DC gain of the lag controller design,  $a_0 = 10$  and the high-frequency gain can be expressed as  $G_{hf}(dB) =$

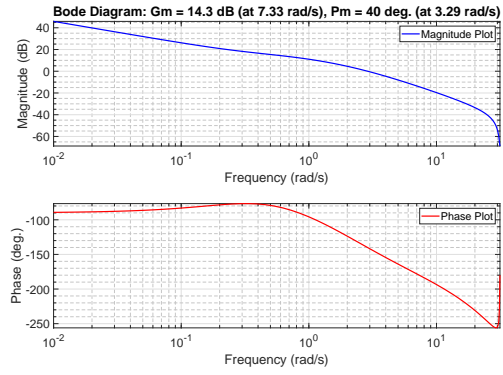


Fig. 4. Bode plot of the compensated open-loop system using phase-lag controller

$20 \log \frac{a_0 \omega_{wp}}{\omega_{w0}}$ . The maximum phase shift lies between 0 and -90 deg. which depends on the ratio  $\omega_{w0}/\omega_{wp}$ . In this paper, the controller is designed for 40 deg. phase margin and the cross-over or phase margin frequency for this design is selected as  $\omega_{wc} = 3.29 \text{ rad/s}$ . Here  $\omega_{w0} = 0.1\omega_{wc}$ , and  $\omega_{wp} = \frac{\omega_{w0}}{a_0 |G_d(j\omega_{wc})|}$ . The design approximates that the controller introduces 5 deg. phase lag to the system and  $|D(j\omega_{wc})G_d(j\omega_{wc})| = 1$ . The lag controller implies that  $\omega_{w0} = 0.3290 < \omega_{wp} = 2.3979$  and the compensating phase angle,  $\phi_m = (-180 + 5 + 40) = -135$  deg. The controller transfer function is  $D_{lag}(z) = \frac{66.15z - 64.01}{z - 0.7859}$ . Fig. 4 presents the Bode plot of the lag-compensated open loop system. It can be observed that the phase margin of the compensated plant is  $P_m = 40$  deg. at  $3.29 \text{ rad/s}$  and the gain margin is  $G_m = 14.3$  dB. The phase-lag controller reduces the phase margin by  $(75.7 - 40) = 35.7$  deg.

### IV. PHASE-LEAD CONTROLLER DESIGN

Again, the DC gain of the phase-lead controller,  $a_0 = 10$  and in this paper, the controller is designed for 40 deg. phase margin and the cross-over or phase margin frequency for this design is selected as  $\omega_{wc} = 2.5 \text{ rad/s}$ . The lead controller design approach yields to

$$D(j\omega_{wc})G_d(j\omega_{wc}) = 1 \angle (180 + \phi_{pm}), |D(j\omega_{wc})| = \frac{1}{|G_d(j\omega_{wc})|} \quad (3)$$

here  $\phi_{pm}$  is the desired phase margin and

$$D(w) = a_0 \frac{1 + w/(a_0/a_1)}{1 + w/(b_1)-1} \quad (4)$$

where  $\omega_{w0} = \frac{a_0}{a_1}$  and  $\omega_{wp} = \frac{1}{b_1}$ . The angle associated with the controller can be expressed as

$$\theta_r = \angle D(j\omega_{wc}) = 180 + \phi_{pm} - \angle G_d(j\omega_{wc}) \quad (5)$$

According to [1], it can be evaluated that

$$a_1 = \frac{1 - a_0 |G_d(j\omega_{wc})| \cos \theta_r}{\omega_{wc} |G_d(j\omega_{wc})| \sin \theta_r}, b_1 = \frac{\cos \theta_r - a_0 |G_d(j\omega_{wc})|}{\omega_{wc} \sin \theta_r} \quad (6)$$

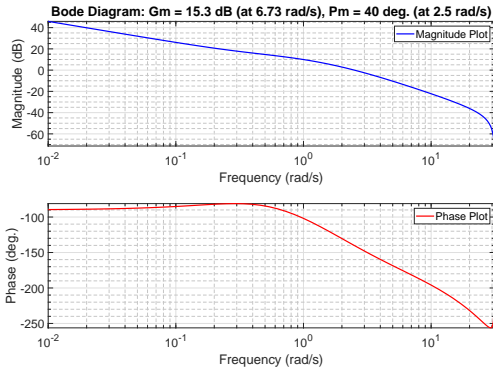


Fig. 5. Bode plot of the compensated open-loop system using phase-lead controller

In the design procedure,  $\omega_{wc}$  is selected to satisfy the constraints:  $\angle G_d(j\omega_{wc}) < 180 + \phi_{pm}$ ;  $|D(j\omega_{wc})| > a_0$ ,  $|G_d(j\omega_{wc})| < \frac{1}{a_0}$ ;  $b_1 > 0$  and  $\cos \theta_r > a_0 |G_d(j\omega_{wc})|$ . The lead controller implies that  $\omega_{w0} = 0.3641 < \omega_{wp} = 1.9603$ . The calculated design parameters:  $a_1 = 27.4649$ ,  $b_1 = 0.5101$ ,  $\theta_r = 389.8149$  deg. and  $\cos \theta_r = 0.9671$ . The controller transfer function is  $D_{lead}(z) = \frac{49.927(z-0.9642)}{(z-0.8251)}$ . Fig. 5 presents the Bode plot of the lead-compensated open loop system. It can be implied that the phase margin of the compensated plant is  $P_m = 40$  deg. at  $2.5 \text{ rad/s}^{-1}$  and the gain margin is  $G_m = 15.3$  dB. The phase-lead controller reduces the phase margin by  $(75.7 - 40) = 35.7$  deg.

#### V. PROPORTIONAL-INTEGRAL (PI) CONTROLLER DESIGN

The PI controller transfer function can be expressed as  $D(w) = K_P + \frac{K_I}{w} = K_I \frac{1+w/\omega_{w0}}{w}$ , here  $\omega_{w0} = K_I/K_P$ . However, the discrete transfer function of a PI controller can be expressed as  $D(z) = K_P + K_I \frac{T}{2} \frac{z+1}{z-1}$ , and the controller frequency response is

$$D(j\omega_w) = K_P - j \frac{K_I}{\omega_w} = |D(j\omega_w)| e^{j\theta_r} \quad (7)$$

At the cross-over frequency, the controller yields to

$$D(j\omega_{wc})G_d(j\omega_{wc}) = 1 \angle (-180 + \phi_{pm}) \quad (8)$$

At the cross-over frequency  $0.8 \text{ rad/s}^{-1}$  in this work,

$$K_P - j \frac{K_I}{\omega_{wc}} = |D(j\omega_{wc})| (\cos \theta_r + j \sin \theta_r) \quad (9)$$

However, the phase angle associated with the controller is

$$\theta_r = -180 + \phi_{pm} - \angle G_d(j\omega_{wc}) \quad (10)$$

The coefficients can be expressed as

$$K_P = \frac{\cos \theta_r}{|G_d(j\omega_{wc})|}, K_I = -\frac{\omega_{wc} \sin \theta_r}{|G_d(j\omega_{wc})|} \quad (11)$$

The controller transfer function is calculated as

$$D_{PI}(z) = \frac{5.839z - 5.823}{z - 1} \quad (12)$$

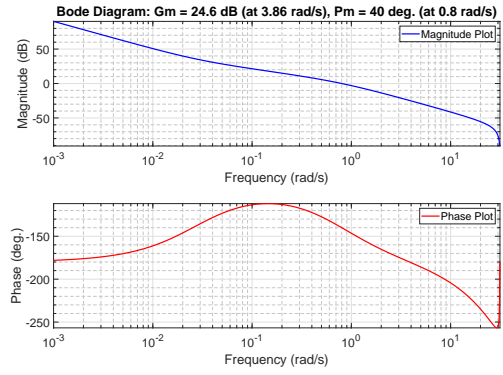


Fig. 6. Bode plot of the compensated open-loop system using proportional-integral (PI) controller

The design parameters are:  $\theta_r = 357.9840$  deg.,  $K_P = 5.8307$  and  $K_I = 0.1642$ . Fig. 6 presents the Bode plot of the PI-compensated open loop system. The phase margin of the compensated plant is  $P_m = 40$  deg. at  $0.8 \text{ rad/s}^{-1}$  and the gain margin is  $G_m = 24.6$  dB. The PI controller reduces the phase margin by  $(75.7 - 40) = 35.7$  deg.

#### VI. PROPORTIONAL-INTEGRAL-DERIVATIVE (PID) CONTROLLER DESIGN

The PID controller transfer function can be expressed as  $D(w) = K_P + \frac{K_I}{w} + K_D w$ . The discrete transfer function of a PID controller can be expressed as  $D(z) = K_P + K_I \frac{T}{2} \frac{z+1}{z-1} + K_D \frac{z-1}{Tz}$ . The controller frequency response is

$$D(j\omega_w) = K_P + j(K_D \omega_w - \frac{K_I}{\omega_w}) = |D(j\omega_w)| e^{j\theta_r} \quad (13)$$

At the cross-over frequency  $1.95 \text{ rad/s}^{-1}$  in this design procedure,

$$K_P + j(K_D \omega_{wc} - \frac{K_I}{\omega_{wc}}) = |D(j\omega_{wc})| (\cos \theta_r + j \sin \theta_r) \quad (14)$$

From the above equations, it can be derived as

$$K_P = \frac{\cos \theta_r}{|G_d(j\omega_{wc})|}, K_D \omega_{wc} - \frac{K_I}{\omega_{wc}} = \frac{\sin \theta_r}{|G_d(j\omega_{wc})|} \quad (15)$$

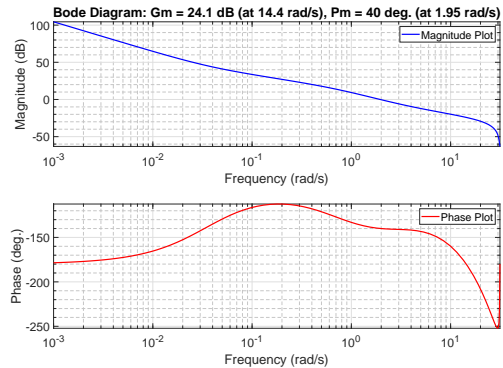


Fig. 7. Bode plot of the compensated open-loop system using proportional-integral-derivative (PID) controller

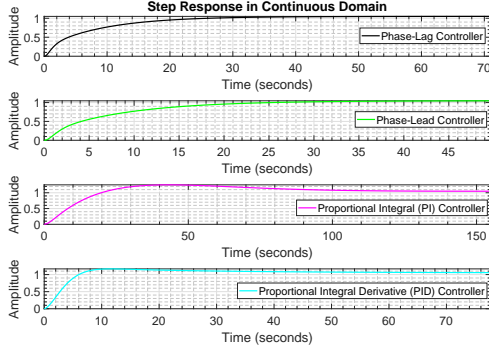


Fig. 8. Step response of the compensated closed-loop system in continuous time domain using different controllers

As a design consideration, adding a pole in the derivative term modifies the controller transfer function as

$$D(w) = K_P + \frac{K_I}{w} + \frac{K_D w}{1 + (T/2)w} \quad (16)$$

However, the modified frequency response is

$$D(j\omega_w) = K_P - j\frac{K_I}{\omega_w} + \frac{K_D j\omega_w}{1 + j\omega_w(T/2)} \quad (17)$$

which yields to

$$\left[ K_P + \frac{K_D \omega_{wc}^2 (2/T)}{(2/T)^2 + \omega_{wc}^2} \right] + j \left[ \frac{K_D \omega_{wc} (2/T)^2}{(2/T)^2 + \omega_{wc}^2} - \frac{K_I}{\omega_{wc}} \right] = K_R + jK_C \quad (18)$$

Here  $K_R = \frac{\cos \theta_r}{|G_d(j\omega_{wc})|}$  and  $K_C = \frac{\sin \theta_r}{|G_d(j\omega_{wc})|}$ . Thereby, it can be concluded that

$$K_P + \frac{K_D \omega_{wc}^2 (2/T)}{(2/T)^2 + \omega_{wc}^2} = \frac{\cos \theta_r}{|G_d(j\omega_{wc})|} \quad (19)$$

and

$$\frac{K_D \omega_{wc} (2/T)^2}{(2/T)^2 + \omega_{wc}^2} - \frac{K_I}{\omega_{wc}} = \frac{\sin \theta_r}{|G_d(j\omega_{wc})|} \quad (20)$$

The controller transfer function is calculated as

$$D_{PID}(z) = \frac{81.51z^2 - 139.5z + 58.07}{z^2 - z} \quad (21)$$

The controller parameters are  $K_I = 0.85$ ,  $K_D = 5.8069$  and  $K_P = 23.3942$ , respectively. The angle associated with the controller is  $\theta_r = 383.7620$  deg. Fig. 7 presents the Bode plot of the PID-compensated open loop system. The phase margin of the compensated plant is  $P_m = 40$  deg. at  $1.95 \text{ rads}^{-1}$  and the gain margin is  $G_m = 24.1$  dB. The PID controller reduces the phase margin by  $(75.7 - 40) = 35.7$  deg.

## VII. STEP RESPONSE CHARACTERISTICS

The single-joint robot arm manipulator in this paper has an input of  $V_{in} = 0.07u(t)$ ; where  $u(t)$  is the unit step function. Fig. 8 presents the scaled step response of the compensated closed loop system in continuous time domain for the digital controllers. However, Table I shows the step response characteristics of the controllers for comparative

TABLE I  
STEP RESPONSE CHARACTERISTICS OF THE CONTROLLERS

Characteristics	Lag	Lead	PI	PID
Steady-State Error	0	0	0	0
Percent Overshoot (%)	0	0	19.1	11.6
Rise Time (s)	18.4	17.9	15.5	4.6
Settling Time (s)	34.1	33	106	51.9

analysis. The steady-state error for all the controllers is found as zero. The phase-lag and phase-lead controllers produce zero percent overshoot. However, the rise time for the PID controller is the lowest among all, whereas the phase-lead controller produces the lowest settling time.

## VIII. CONCLUSION

This paper presents design and performance analysis of digital controllers - phase-lag, phase-lead, PI and PID for a single DOF robot arm manipulator. The phase margin for the compensated system is selected as 40 deg and cross-over frequency is the prime criterion in the design procedure. However, the controllers are designed and implemented in both discrete (z-domain or actual digital) and continuous (warped s-domain or w-plane) time domains. For performance assessments, MATLAB ® simulations are carried out for open-loop Bode plots and closed loop step response characteristics.

## REFERENCES

- [1] D. Chowdhury, "Design and Performance Analysis of Digital Controllers in Discrete and Continuous Time Domains for a Robot Control System," *Global J. Research Eng.*, vol. 18, no. 3, pp. 29–41, 2018.
- [2] S. A. Fattah, D. Chowdhury, M. Z. Haider, M. Sarkar, M. Refat, G. Rabbi, S. B. Masud and C. Shahnaz, "Dynamic map generating rescuer offering surveillance robotic system with autonomous path feedback capability," in *Proc. IEEE Region 10 Humanitarian Technology Conf. (R10-HTC)*, Philippines, 2015, pp. 1–6.
- [3] A. Bhattacharjee, A. I. Khan, M. Z. Haider, S. A. Fattah, D. Chowdhury, M. Sarkar and C. Shahnaz, "Bangla voice controlled robot for rescue operation in noisy environment," in *Proc. IEEE Region 10 Conf. (TENCON)*, Singapore, 2016, pp. 3284–3288.
- [4] S. A. Fattah, M. Z. Haider, D. Chowdhury, M. Sarkar, R. I. Chowdhury, M. S. Islam, R. Karim, A. Rahi and C. Shahnaz, "An aerial landmine detection system with dynamic path and explosion mode identification features," in *Proc. IEEE Global Humanitarian Technology Conf. (GHTC)*, USA, 2016, pp. 745–752.
- [5] D. Chowdhury, M. Sarkar, M. Z. Haider, S. A. Fattah and C. Shahnaz, "Design and implementation of a cyber-vigilance system for anti-terrorist drives based on an unmanned aerial vehicular networking signal jammer for specific territorial security," in *Proc. IEEE Region 10 Humanitarian Technology Conf. (R10-HTC)*, Bangladesh, 2017, pp. 444–448.
- [6] F. A. Salem, "Modeling, Simulation and Control Issues for a Robot ARM; Education and Research," *Int. J. Intelligent Syst. and Applicat.*, vol. 4, pp. 26–39, 2014.
- [7] R. Agrawal, K. Kabiraj and R. Singh, "Modeling a Controller for an Articulated Robotic Arm," *Intelligent Control and Automation*, vol. 3 pp. 207–210, 2012.
- [8] H.- S. Kim and J.- B. Song, "Multi-DOF Counterbalance Mechanism for a Service Robot Arm," *IEEE/ASME Trans. Mechatronics*, vol. 19, no. 6, pp. 1756–1763, 2014.
- [9] K. Lee, J. Lee, B. Woo, J. Lee, Y.- J. Lee and S. Ra, "Modeling and Control of a Articulated Robot Arm with Embedded Joint Actuators," in *Proc. Int. Conf. Inform. and Commun. Technology Robotics (ICT-ROBOT)*, South Korea, 2018, pp. 1–4.
- [10] A. D. Shakibjoo and M. D. Shakibjoo, "2-DOF PID with reset controller for 4-DOF robot arm manipulator," in *Proc. Int. Conf. Advanced Robotics and Intelligent Syst. (ARIS)*, Taiwan, 2015, pp. 1–6.